

1 **Building a machine learning surrogate model for wildfire activities within a global earth**
2 **system model**

3 Qing Zhu^{1,*}, Fa Li^{1,2}, William J. Riley¹, Li Xu³, Lei Zhao⁴, Kunxiaoqia Yuan^{1,2}, Huayi Wu²,
4 Jianya Gong⁵, James Randerson³

5
6 ¹ Climate and Ecosystem Sciences Division, Climate Sciences Department, Lawrence Berkeley
7 National Laboratory, Berkeley, CA, USA

8 ² State Key Laboratory of Information Engineering in Surveying, Mapping and Remote Sensing,
9 Wuhan University, Wuhan, China

10 ³ Department of Earth System Science, University of California Irvine, Irvine, CA, USA

11 ⁴ Department of Civil and Environmental Engineering, University of Illinois Urbana-Champaign,
12 Champaign, IL, USA

13 ⁵ School of Remote Sensing and Information Engineering, Wuhan University, Wuhan, China

14 *Correspondence to Qing Zhu (qzhu@lbl.gov)

15 **Abstract**

16 Wildfire is an important ecosystem process, influencing land biogeophysical and
17 biogeochemical dynamics and atmospheric composition. Fire-driven loss of vegetation cover, for
18 example, directly modifies the surface energy budget as a consequence of changing albedo,
19 surface roughness, and partitioning of sensible and latent heat fluxes. Carbon dioxide and
20 methane emitted by fires contribute to a positive atmospheric forcing, whereas emissions of
21 carbonaceous aerosols may contribute to surface cooling. Process-based modeling of wildfires in
22 earth system land models is challenging due to limited understanding of human, climate, and
23 ecosystem controls on fire number, fire size, and burned area. Integration of mechanistic wildfire
24 models within Earth system models requires careful parameter calibration, which is
25 computationally expensive and subject to equifinality. To explore alternative approaches, **we**
26 **present a deep neural network (DNN) scheme that surrogates the process-based wildfire model**
27 **with the Energy Exascale Earth System Model (E3SM) interface.** The DNN wildfire model
28 accurately simulates observed burned area with over 90% higher accuracy with a large reduction
29 in parameterization time compared with the current process-based wildfire model. **The surrogate**
30 **wildfire model successfully captured the observed monthly regional burned area during**
31 **validation period 2011 to 2015 (coefficient of determination, $R^2 = 0.93$).** Since the DNN wildfire
32 model has the same input and output requirements as the E3SM process-based wildfire model,
33 our results demonstrate the applicability of machine learning for high accuracy and efficient
34 large-scale land model development and predictions.

35 1. Introduction

36 Wildfires burn ~500 million hectares of vegetated land surface each year, which
37 significantly modifies the physical properties and biogeochemical cycles of terrestrial
38 ecosystems [Andela *et al.*, 2017; Bond-Lamberty *et al.*, 2007; Pellegrini *et al.*, 2018; Randerson
39 *et al.*, 2006]. Living vegetation biomass, surface litter, and coarse woody debris are directly
40 combusted and removed by wildfire [Harden *et al.*, 2006; Walker *et al.*, 2019]. It has been
41 suggested that global forest would double if fire were eliminated [Bond *et al.*, 2005; Lasslop *et*
42 *al.*, 2020]. Fire has multiple important consequences for the climate system, including directly
43 releasing greenhouse gases (*e.g.*, CO₂, CH₄) [Kasischke and Bruhwiler, 2002; Ross *et al.*, 2013]
44 and aerosols [Jiang *et al.*, 2020]; changing land surface albedo and energy budgets [French *et*
45 *al.*, 2016; Rother and De Sales, 2020] and land-atmosphere exchanges of heat, mass, and
46 momentum [Chambers and Chapin, 2002]; limiting plant transpiration and regional water
47 recycling [Brando *et al.*, 2020; Holden *et al.*, 2018]; and reshaping forest composition
48 [Mekonnen *et al.*, 2019]. In addition, biomass burning emits a large amount of fine particulate
49 matter that contributes to about 30% of cloud condensation nuclei globally [Day, 2004]. Soil
50 organic matter decomposition, nitrogen mineralization, and the richness and diversity of soil
51 fungal communities [Oliver *et al.*, 2015] could also be influenced by wildfire through modifying
52 litter substrate supply and degraded enzymatic activities [Bowd *et al.*, 2019; Holden *et al.*, 2018;
53 Pellegrini *et al.*, 2018; Pellegrini *et al.*, 2020].

54 Climate change and land use activities have jointly affected fire spatial distribution,
55 frequency, and intensity [Andela *et al.*, 2017; Kelley *et al.*, 2019; Xu *et al.*, 2020] since the pre-
56 industrial era. For example, warmer and drier climate conditions enhance fuel aridity and favor
57 fire occurrence in forest ecosystems where fuels have built up over a period of decades and
58 centuries [Abatzoglou and Williams, 2016; Williams *et al.*, 2019]. Even if annual precipitation
59 does not decline, redistribution of precipitation towards wet season extreme rainfall events could
60 contribute to longer dry periods and thus more severe fire activity [Xu *et al.*, 2020]. Human
61 activities often shape wildfire activity through regulating patterns of ignition and fire occurrence
62 (*e.g.*, powerline ignition) [Keeley and Syphard, 2018] and suppressing wildfire activity by means
63 of land fragmentation, fire management, and livestock grazing [Andela *et al.*, 2017]. In
64 California, fire density is highly associated with population density and the distance to the
65 wildland urban interface (WUI) [Syphard *et al.*, 2007]. At the global scale, along gradients of

66 increasing population density, fire frequency initially increases by up to 20% and then gradually
67 declines in more densely populated areas [Knorr et al., 2014].

68 Although global wildfire burned area has declined over the recent two decades [Andela et
69 al., 2017], many vulnerable ecosystems and geographic regions have experienced significant
70 increases in wildfire activity [Abatzoglou and Williams, 2016; Walker et al., 2019] resulting in
71 large losses of natural resources and economic assets [Papakosta et al., 2017; Stephenson et al.,
72 2013]. Over western U.S. forests, wildfire has dramatically increased, costing billions of dollars
73 each year and gaining wide public attention. This regional wildfire increase is mainly driven by
74 concurrent increases of spring temperature and declining snowpack [Westerling et al., 2006],
75 mid-summer increases in vapor pressure deficit [Williams et al., 2019], and increases in drought
76 stress during fall [Goss et al., 2020]. The enhancement of wet and dry oscillations favors initial
77 vegetation growth and subsequent wildfire activity [Heyerdahl et al., 2002; Saha et al., 2019].

78 Wildfire models have played an important role in many aspects of wildfire research,
79 including monitoring fire spread [Finney, 1998; Radke et al., 2019], analyzing controllers of
80 wildfire short-term and long-term variability [Kelley et al., 2019], predicting severity of the
81 upcoming fire seasons [Preisler and Westerling, 2007] and climate-scale fire variability
82 [Girardin and Mudelsee, 2008; Yue et al., 2013], and understanding the complex climate-
83 wildfire-ecosystem feedbacks [Clark et al., 2004; Mekonnen et al., 2019; Zou et al., 2020]. Two
84 types of wildfire models are widely used: process-based models and data-driven statistical
85 models. Process-based wildfire models consider detail processes related to natural fire ignition
86 [Prentice and Mackerras, 1977], anthropogenic ignition [Venevsky et al., 2002], fire spread and
87 duration [Thonicke et al., 2010], fire suppression [Lenihan and Bachelet, 2015], and fire mass
88 and heat fluxes [F Li et al., 2012]. Process-based wildfire models have been widely used in
89 dynamic vegetation models and coupled earth system models (ESMs) with various complexities
90 of parameterization [Fang Li et al., 2019; Rabin et al., 2017]. As more and more detailed fire
91 processes are considered and parameterized, structural and parametric uncertainties may increase
92 due to incomplete representation of individual processes and imperfect mathematical formulation
93 [Riley and Thompson, 2017]. **Historically, data-driven models were often used for fire behavior
94 modeling and aim to track the ignition, spread, duration, and extinction of individual fires
95 [Finney, 1998; Radke et al., 2019] at fine spatial and temporal scales. This group of models are
96 more relevant to operational fire research. While process-based wildfire models in the context of**

97 global vegetation models or earth system land models focuses on the gridcell aggregated fire
98 burned area dynamics that are more relevant to researches on large scale patterns and climate
99 scale predictions [Fang Li et al., 2019; Rabin et al., 2017]. This study particularly focuses on the
100 second category of wildfire models.

101 Although explicit processes are simulated, the accuracy of process-based wildfire models
102 are highly dependent on parameterization, which is computationally expensive [Teckentrup et
103 al., 2018; Zhu and Zhuang, 2014]. Data-driven models, however, directly link the driving
104 variables (e.g., climate factors) to the fire activity using simple statistical models or more
105 sophisticated machine learning techniques, ignoring the explicit processes and feedbacks
106 associated with wildfire [Ganapathi Subramanian and Crowley, 2018; Radke et al., 2019; Tonini
107 et al., 2020]. Through training and validation, statistical representations of wildfire dynamics are
108 learned by models using principles from machine learning. Data-driven wildfire models are
109 diverse in terms of driving variables and model structure. For example, many current machine
110 learning wildfire models rely on remote oceanic dynamics (e.g., sea surface temperature
111 variability) and atmospheric teleconnections to simulate land surface fire activities [Chen et al.,
112 2020; Chen et al., 2011; Yu et al., 2020]. Another group of data-driven wildfire models draws
113 more heavily upon regional climate, plant functional type, and human infrastructure driver
114 variables [Coffield et al., 2019; Sayad et al., 2019].

115 In this study, we develop a machine learning wildfire model using the process
116 representation of wildfire in the Energy Exascale Earth System Model (E3SM) land model
117 (ELMv1) [Zhu et al., 2019], five observationally inferred burned area products [Andela et al.,
118 2019; Giglio et al., 2018; Joshua Lizundia-Loiola et al., 2020; J Lizundia-Loiola et al., 2018;
119 Van Der Werf et al., 2017], and a deep neural network approach [Goodfellow et al., 2016]. We
120 implemented a deep learning model that can better capture the complex and non-linear
121 interactions between controlling factors and wildfire activity. The objectives of this study are to
122 surrogate the wildfire parameterization in ELMv1 with the deep neural network and improve the
123 model simulated wildfire burned area across various fire regions [Giglio et al., 2013].

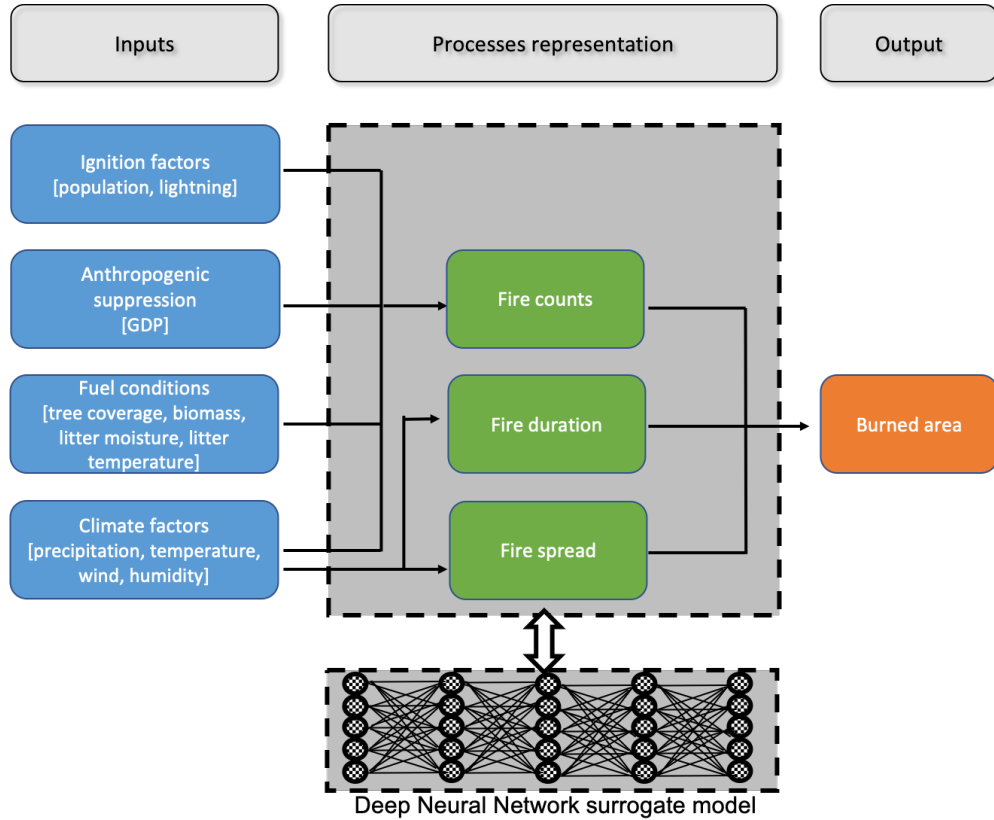
124

125 **2. Methodology**

126 **2.1 ELMv1 wildfire model**

127 The process-based wildfire model in ELMv1 originates from the Community Land
128 Model (CLM4.5) [*F Li et al.*, 2012]; we take this wildfire model as the baseline (hereafter refer
129 to as BASE-Fire). BASE-Fire combines information regarding ignition, fuel conditions, surface
130 climate, and anthropogenic suppression to simulate total burned area based on the fire counts and
131 spread area of each fire (Figure 1). The fire count in BASE-Fire is modeled as the sum of
132 anthropogenic ignition and natural ignition, where the latter is proportional to lightning density
133 [*Prentice and Mackerras*, 1977] and the former is determined by population density [*Venevsky et*
134 *al.*, 2002]. Human activity may also intentionally suppress wildfire occurrence if the fire is
135 detected at early stage. For example, developed regions with high population density and gross
136 domestic product are less likely to use fire to remove surface biomass. On the other hand,
137 developed regions more likely suppress fire given more effective fire management policy and
138 suppression capability. Fire count is also affected by surface fuel availability (aboveground
139 biomass) and fuel combustibility (relative humidity, topsoil temperature and moisture). The fire
140 spread area in BASE-Fire is modeled as an elliptical shaped region controlled by wind speed and
141 fuel wetness (using topsoil (0 – 15 cm) moisture as a proxy). The fire duration is set to be one
142 day based on a study that reported years 2001-2004 mean global fire persistence [*Giglio et al.*,
143 2006a]. BASE-Fire also does not explicitly consider roads, rivers, and firefighting activity
144 [*Arora and Boer*, 2005].

145



146

147 **Figure 1.** Schematic representation of the ELMv1 process-based BASE-Fire model and the
 148 components to be surrogated with the Deep Neural Network (DNN) model (dark grey).

149

150 2.2 Deep neural network wildfire surrogate model

151 We developed the new fire model in two steps: (1) surrogating BASE-Fire with a deep
 152 neural network (DNN) approach and (2) **improving that surrogate model using five**
 153 **observationally inferred burned area products (Table S1)**. First, we surrogated BASE-Fire with a
 154 DNN approach (hereafter refer to as DNN-Fire) that uses the same input and output variables as
 155 BASE-Fire but treats the explicit intermediate processes (*e.g.*, ignition, fire spread) as latent
 156 variables coded by hidden layers in the DNN (Figure 1). DNN-Fire was developed with five
 157 hidden layers and five neurons in each layer for burned area simulation. The DNN approach uses
 158 a fully-connected feedforward neural network [*Schmidhuber, 2015*] that comprises input, hidden,
 159 and output layers:

$$h_1 = f_1(W_1 I + b_1) \quad (1)$$

$$h_2 = f_2(W_2 h_1 + b_2) \quad (2)$$

$$h_3 = f_3(W_3 h_2 + b_3) \quad (3)$$

$$h_4 = f_4(W_4 h_3 + b_4) \quad (4)$$

$$h_5 = f_5(W_5 h_4 + b_5) \quad (5)$$

$$O = f_6(W_6 h_5 + b_6) \quad (6)$$

160 where I denotes the input layer (*e.g.*, climate factors) with 11 neurons, each corresponding to an
 161 input variable listed in Table 1. h_1 , h_2 , h_3 , h_4 , and h_5 are five hidden vectors that are calculated
 162 with two steps. First is a linear combination of previous layers' input vector (h) and the trainable
 163 weight parameter matrix [W_1 , W_2 , W_3 , W_4 , W_5 , W_6], considering biases b_1 , b_2 , b_3 , b_4 , b_5 , and b_6 .
 164 Then, nonlinear activation functions f_1 , f_2 , f_3 , f_4 , f_5 , and f_6 . are applied to the output from the
 165 previous step. In this study we used *softplus* as the activation function [Zheng *et al.*, 2015] that is
 166 a non-linear transformation of input signals. O denotes the output layer that summarize the latent
 167 variables from the last hidden layer (h_5) and calculate burned area.

168 **Table 1.** Input and output variables of ELMv1 BASE-Fire and surrogate DNN-Fire models

Variable category	Variable name	Data source and reference
<i>Input variables</i>		
Fuel conditions	Tree coverage	LUH2 [Hurtt <i>et al.</i> , 2020]
	Fuel load	ELMv1 total biomass [Zhu and Riley, 2015; Zhu <i>et al.</i> , 2019]
	Fuel wetness	ELMv1 topsoil moisture [Zhu and Riley, 2015; Zhu <i>et al.</i> , 2019]
	Fuel temperature	ELMv1 topsoil temperature [Zhu and Riley, 2015; Zhu <i>et al.</i> , 2019]
Climate factors	Precipitation	GSWP3 [Dirmeyer <i>et al.</i> , 2006]
	Near surface temperature	GSWP3 [Dirmeyer <i>et al.</i> , 2006]
	Wind speed	GSWP3 [Dirmeyer <i>et al.</i> , 2006]
	Relative humidity	GSWP3 [Dirmeyer <i>et al.</i> , 2006]
Ignition	Population density	[Dobson <i>et al.</i> , 2000]
	Lightning frequency	NASA-LIS/OTD [Cecil <i>et al.</i> , 2014]
Anthropogenic suppression	GDP	[van Vuuren <i>et al.</i> , 2007]
	Population density	[Dobson <i>et al.</i> , 2000]

<i>output variable</i>	
Burned area	ELMv1 percentage burned area [<i>Zhu and Riley, 2015; Zhu et al., 2019</i>]

169

170 Second, we improved the surrogate DNN-Fire by fine-tuning the weight parameters using
 171 observations (hereafter refer to **DNN-Fire-OBS**). Between 2001 and 2010, we initialized
 172 DNN-Fire-OBS’s weight parameters (W_1 , W_2 , W_3 , W_4 , W_5 , and W_6) using results from DNN-Fire,
 173 replaced the BASE-Fire burned area by **the ensemble mean of five observationally inferred**
 174 **burned area products including GFEDv4s [*Van Der Werf et al., 2017*], Fire_CCI51 [*Joshua***
 175 ***Lizundia-Loiola et al., 2020*], Fire_CCILT11 [*J Lizundia-Loiola et al., 2018*], MODIS MCD64**
 176 ***[Giglio et al., 2018]*, and Fire_Atlas [*Andela et al., 2019*] (Table S1)**, and adjusted weight
 177 parameters until the model best reproduced the observed burned area. This two-step approach
 178 will also allow rapid parameterization of the Fire model as new fire data and baseline fire model
 179 results become available. DNN-Fire-OBS can be more easily generalized since BASE-Fire
 180 provides explicit physical guidance and a larger-than-observation input and output feature space
 181 for development of the machine learning fire model.

182 **2.3 Model setup and simulation protocol**

183 We ran ELMv1 with BASE-Fire at 1.9° by 2.5° spatial resolution [*Zhu et al., 2020; Zhu*
 184 *et al., 2016*] to generate training and testing datasets for the DNN wildfire model. BASE-Fire
 185 was first spun up for 600 years with accelerated soil decomposition followed by 200 years
 186 regular spinup with regular soil decomposition [*Koven et al., 2013*]. The spinup simulations were
 187 forced with constant atmospheric CO₂ concentration (285 ppmv) and 1901-1920 repeated
 188 climate forcing from GSWP3 (Global Soil Wetness Project) [*Dirmeyer et al., 2006*]. The purpose
 189 of the spinup was to initialize ecosystem carbon pools and stabilize plant and soil carbon and
 190 water fluxes. Restarting from the “spinup” conditions, a transient simulation was then conducted
 191 from 1901 to 2015 with GSWP3 transient climate forcing, atmospheric CO₂ concentrations, and
 192 nitrogen and phosphorus deposition [*Lamarque et al., 2005; Mahowald et al., 2008*]. Wildfire
 193 associated variables were selected for output with a monthly temporal resolution (Table 1).

194 BASE-Fire output from years 1981 to 2010 were used to train, test, and fine-tune
 195 DNN-Fire. We developed 14 region-specific models, corresponding to 14 widely used GFED
 196 regions. For each region, all land gridcells (comprising no fire history, infrequent fire, and

197 repeated fire) were concatenated into one data matrix (where rows consist of the number of
 198 samples and columns of the number of variables). 80% of the data matrix was randomly sampled
 199 for the training dataset and the remaining 20% of the data were reserved for testing. Furthermore,
 200 the random sampling was stratified in order to reduce the risk of sampling, e.g., adjacent high
 201 fire grid cells. All grid cells were first divided into three “strata”: low burn (0-33% percentile),
 202 median burn (33%-66% percentile), and high burn (67-100% percentile) grid cells based on the
 203 magnitude of the burn. The stratified random sample assured the sampled grid cells for training
 204 and testing had the same ratios of low/medium/high burn, thus eliminating the sampling bias
 205 from spatial autocorrelation [Wang et al., 2012]. In addition to random sampling, we also
 206 investigated the impacts of data choice on the model performance, by sampling the testing
 207 datasets within specific years (e.g., 2001-2002, 2003-2004, 2005-2006, 2007-2008, 2009-2010)
 208 and used the rest of the years for training. We found neglected differences among the models
 209 (Figure S1) indicating the choice of training/testing data years were not impactful. Therefore, we
 210 will discuss the results with stratified random sampling approach as the major results throughout
 211 the paper.

212 All training and testing datasets were normalized to the range [0, 1] with the following
 213 scaler:

$$X = \frac{X - X_{min}}{X_{max} - X_{min}} \quad (7)$$

214 where X is the variable vector of interest and X_{min} and X_{max} are minimum and maximum values of
 215 X , respectively. During the training stage, we randomly initialized the weighting parameters (Eq.
 216 1-6) and optimized them using the Adaptive Moment Estimation method [Kingma and Ba,
 217 2014], which is a variant of the gradient descent optimization method but considers adaptive
 218 learning rate and momentum-like exponentially decaying gradients. The parameter optimization
 219 aimed to minimize a mean squared error cost function:

$$J = \frac{1}{n} \sum_{i=1}^n (y_i^{DNN} - y_i^{BASE})^2 \quad (8)$$

220 where y_i^{DNN} and y_i^{BASE} are DNN-Fire and BASE-Fire generated burned area, respectively. Cost
 221 function J summarizes the overall magnitude of the error between the surrogate DNN-Fire and
 222 BASE-Fire. We then evaluated model performance using metrics of mean absolute error (Eqn.
 223 9), Pearson correlation (Eqn. 10), and coefficient of determination (Eqn. 11).

$$MAE = \frac{1}{n} \sum_{i=1}^n |y_i^{DNN} - y_i^{BASE}| \quad (9)$$

225
$$p = \frac{\text{covariance}(y^{DNN}, y^{BASE})}{\text{variance}(y^{DNN})\text{variance}(y^{BASE})} \quad (10)$$

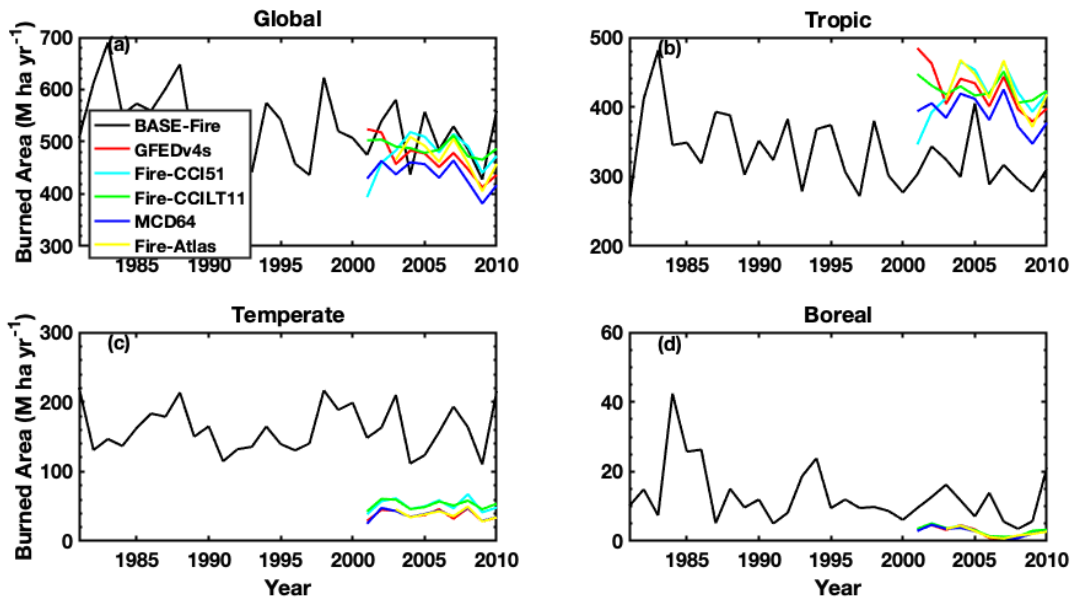
226
$$R^2 = 1 - \frac{\sum_{i=1}^n (y_i^{DNN} - y_i^{BASE})^2}{\sum_{i=1}^n (y_i^{BASE} - y_{mean}^{BASE})^2} \quad (11)$$

227

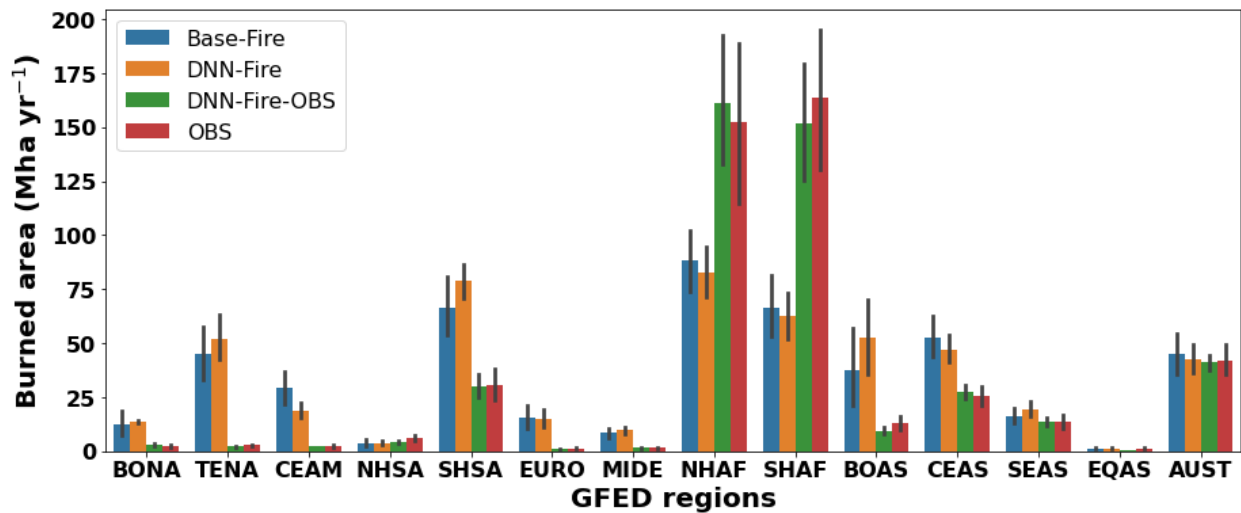
228 3. Results and discussion

229 3.1 Evaluation of wildfire surrogate model

230 BASE-Fire performed reasonably well for total global burned area (508 ± 53 Mha yr⁻¹
231 (million hector per year) between years 2001 and 2010 compared with the observational long-
232 term average of 424~484 Mha yr⁻¹; Figure 2, Table S1). BASE-Fire also captured the global
233 declining trend of wildfire burned area over this time period, attributed to a decrease in tropical
234 fires [Andela et al., 2017]. At the regional scale, however, BASE-Fire underestimated tropical
235 (S23.5° - N23.5°) burned area and overestimated temperate (N23.5° - N67.5°) and boreal (N67.5°
236 above) burned area (Figure 2). Large spatial heterogeneity existed for BASE-Fire regional bias.
237 For example, over tropical GFED regions, BASE-Fire overestimated wildfire burned area over
238 Southern Hemisphere South America (SHSA), but underestimated wildfire burned area over both
239 Southern and Northern Hemisphere Africa regions (SHAF and NHAF), despite an overall
240 underestimation over the tropical region (Figure 3). In contrast, consistent overestimation
241 occurred over all temperate GFED regions. For example, wildfire burned was overestimated by
242 about a factor of 16 (~1 versus 16 Mha yr⁻¹) over the Europe GFED region (EURO) (Figure 3).
243 Although there is room to improve BASE-Fire performance, the parameterization would involve
244 large ensemble simulations and computational resources. Instead, we first used BASE-Fire
245 generated data as training and testing datasets to parameterize DNN-Fire, then we fine-tuned the
246 DNN-Fire model against observed burned area.



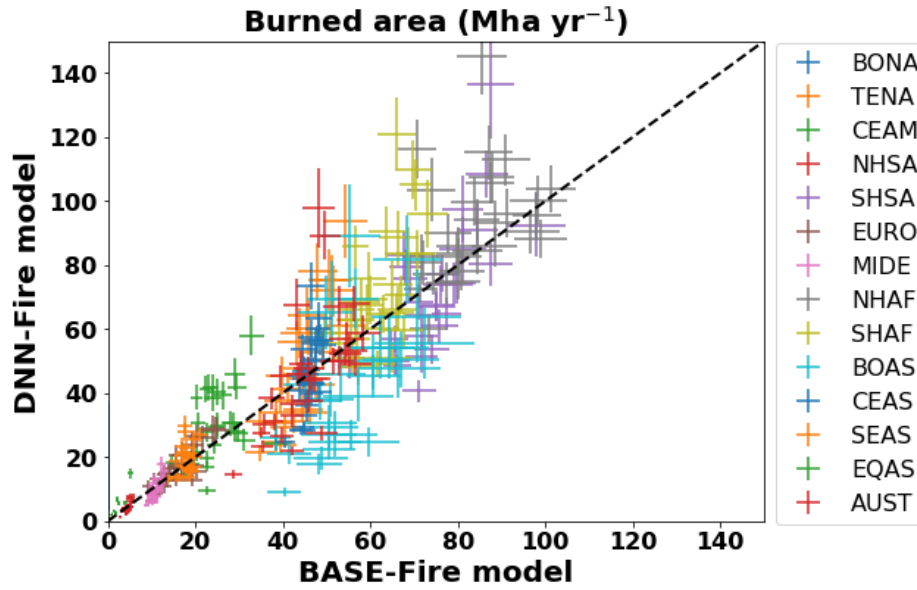
247
 248 **Figure 2.** ELMv1 process-based model (BASE-Fire) simulated and five observationally inferred
 249 burned area products (Table S1) at (a) global scale; (b) Tropical (S23.5° -N23.5°); (c) Temperate
 250 (N23.5° - N 67.5°); and (d) Boreal (north of N 67.5°) regions.
 251



252
 253 **Figure 3.** A comparison of wildfire burned area between estimates from the ELMv1 process-
 254 based model (BASE-Fire), Deep Neural Network wildfire model (DNN-Fire), Deep Neural
 255 Network wildfire model fine-tuned with observed burned area (DNN-Fire-OBS), and
 256 observations over 14 GFED fire regions.
 257

258 Next we parameterized and compared DNN-Fire with BASE-Fire outputs. Using BASE-
259 Fire generated $1.9^\circ \times 2.5^\circ$ resolution datasets of surface fuel conditions (fuel load (vegetation
260 biomass), fuel temperature (topsoil temperature), and fuel wetness (topsoil moisture)) with
261 gridded climate forcing (GSWP3) [Dirmeyer *et al.*, 2006], land use (LUH2 dataset) [Hurtt *et al.*,
262 2020], and social economic [Dobson *et al.*, 2000; van Vuuren *et al.*, 2007] factors, DNN-Fire
263 captured the spatial pattern of BASE-fire predicted wildfire activity (Figure 4, Figure S2).
264 Across all GFED regions, mean absolute error of DNN-Fire was 4.4 Mha yr^{-1} (<1% of total burn
265 area), with median and maximum errors of 1.8 and 13.0 Mha yr^{-1} , respectively (Figure 3).
266 Equatorial Asia (EQAS), Northern Hemisphere South America (NHSA), Central America
267 (CEAS), and Europe (EURO) regions had the lowest DNN-Fire errors (< 1.0 Mha yr^{-1}), while
268 Southern Hemisphere Africa (SHAF), and Boreal Asia (BOAS) had the largest errors (10-13
269 Mha yr^{-1}). Overall, the correlation coefficient between BASE-Fire and DNN-Fire simulated
270 burned area was 0.91 (p value < 0.01) and the coefficient of determination (R^2) was 0.79. Across
271 seasons, DNN-Fire also reasonably captured the BASE-Fire peak fire months (June to October),
272 which were dominated by Southern Hemisphere Africa and Southern Hemisphere South
273 America (Figure 5).

274 By surrogating BASE-Fire, DNN-Fire is expected to have similar biases and
275 uncertainties. The deficiency of BASE-Fire model will propagate to DNN-Fire. In our future
276 work we will overcome such limitation by training multiple DNN-Fire models with ensemble
277 simulations of BASE-Fire models that differ in critical parameters and vary in model structures.
278



279
 280 **Figure 4.** The performance of the Deep Neural Network wildfire model (DNN-Fire), compared
 281 with the original ELMv1 process-based wildfire model (BASE-Fire) over 14 GFED regions
 282 between years 2001 and 2010.

283
 284 **3.2 Calibrating the wildfire surrogate model using observations**

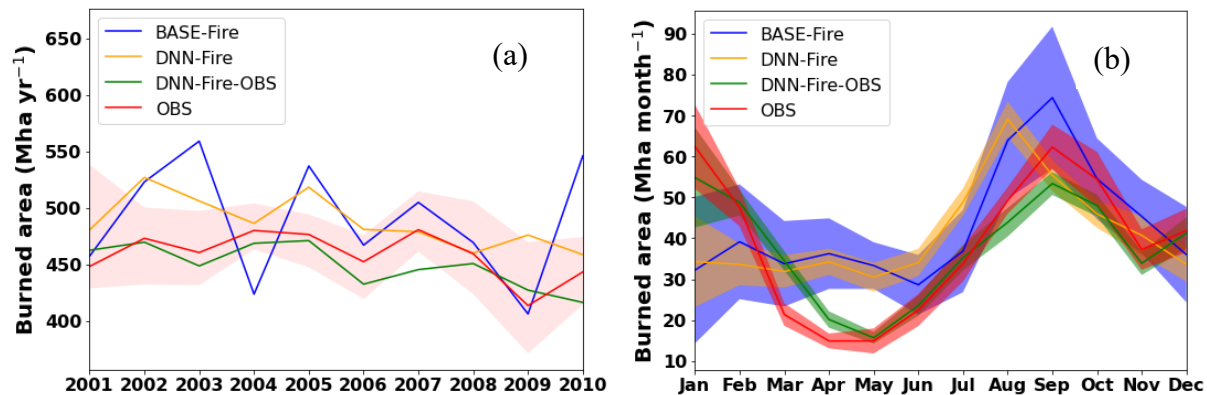
285 Although the global pattern was reasonably captured, BASE-Fire had relatively large
 286 biases in several GFED regions, as discussed above. Since DNN-Fire was trained and validated
 287 only with BASE-Fire generated inputs (*e.g.*, fuel conditions) and outputs (burned area), we
 288 expect that, at best, DNN-Fire would have comparable biases as BASE-Fire. Starting from
 289 DNN-Fire, we further calibrated the model weighting parameters to create DNN-Fire-OBS and
 290 validated DNN-Fire-OBS performance using observed burned area from five existing burned
 291 area products (Table S1) between years 2001 and 2010. The calibration time cost several minutes
 292 with Intel Xeon Phi Processor 7250 processor.

293 Dramatic improvements were found in most of the 14 regions simulated by DNN-Fire-
 294 OBS (Figure 3). Overall, DNN-Fire-OBS simulated global long-term average burned area was
 295 458 Mha yr⁻¹ (compared with observational average 467 Mha yr⁻¹). Averaged across 14 regions,
 296 73% reduction of mean absolute error was achieved by DNN-Fire-OBS, compared with the
 297 BASE-Fire model. Pearson correlation coefficient between the DNN-Fire-OBS simulated and
 298 observational burned area was 0.98 (*p* value < 0.001) with an *R*² of 0.97. Bias reduction was
 299 disproportionately distributed across the GFED regions (Figure 3). For example, severely burned

300 regions, including Southern and Northern Hemisphere Africa (SHAF and NHAF) and Southern
 301 Hemisphere South America (SHSA) greatly benefited from the tuning and their regional biases
 302 were reduced by 88, 65, and 51 Mha yr⁻¹ (or 88%, 89%, 98% reduction), respectively. Although
 303 Temperate Northern America (TENA) and Europe (EURO) wildfire burned area is relatively
 304 small (1-3 Mha yr⁻¹), the impacts of wildfire activity were significant due to their high population
 305 densities. DNN-Fire tended to overestimate the burned area in TENA and EURO by 47 and 13
 306 Mha yr⁻¹, while DNN-Fire-OBS significantly reduced biases in both regions to less than 0.3 Mha
 307 yr⁻¹ (a 97-98%% reduction).

308 BASE-Fire tended to overestimate inter-annual variability (IAV) and had opposite burned
 309 area anomalies between years 2001 and 2005. DNN-Fire dampened BASE-Fire's IAV, but had
 310 systematic overestimation of burned area. DNN-Fire-OBS agreed well with the observed IAV
 311 between years 2001 and 2010 (Figure 5a). The seasonal cycle was also improved in DNN-Fire-
 312 OBS in terms of reducing BASE-Fire's overestimation of burned area during peak fire seasons
 313 (Figure 5b, Figure S3), although we note that DNN-Fire-OBS is biased high during low fire
 314 seasons (March and April).

315



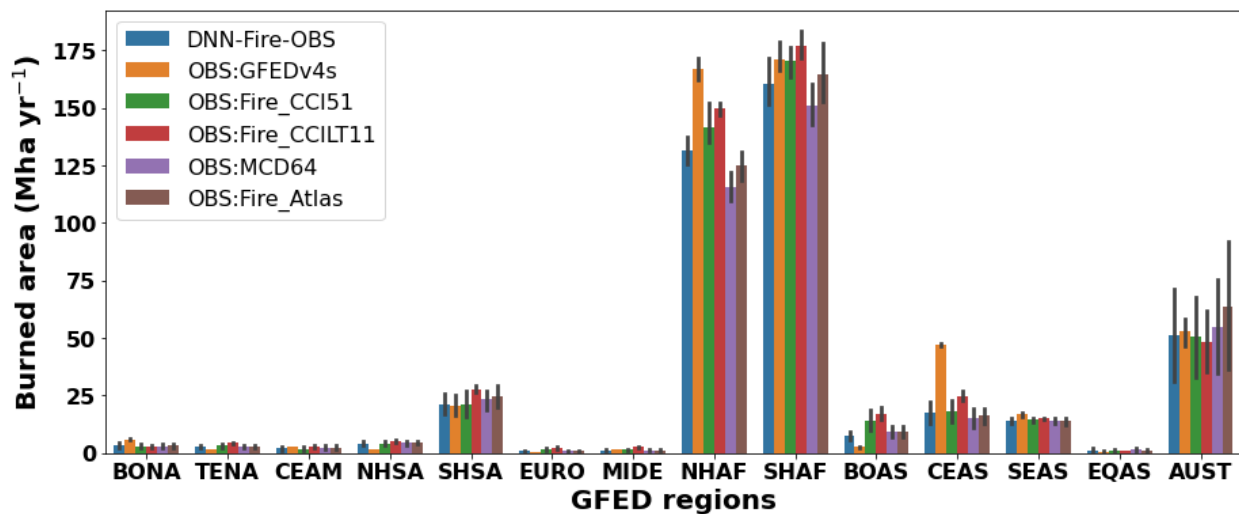
316
 317 **Figure 5.** Inter-annual variation of burned area from years 2001 to 2010 (a) and the averaged
 318 seasonal cycle (b) of burned area estimated by the ELMv1 process-based wildfire model (BASE-
 319 Fire), Deep Neural Network wildfire model (DNN-Fire), Deep Neural Network wildfire model
 320 fine-tuned with observations (DNN-Fire-OBS), and observations.

321

322 3.3 Prognostic simulation and limitations

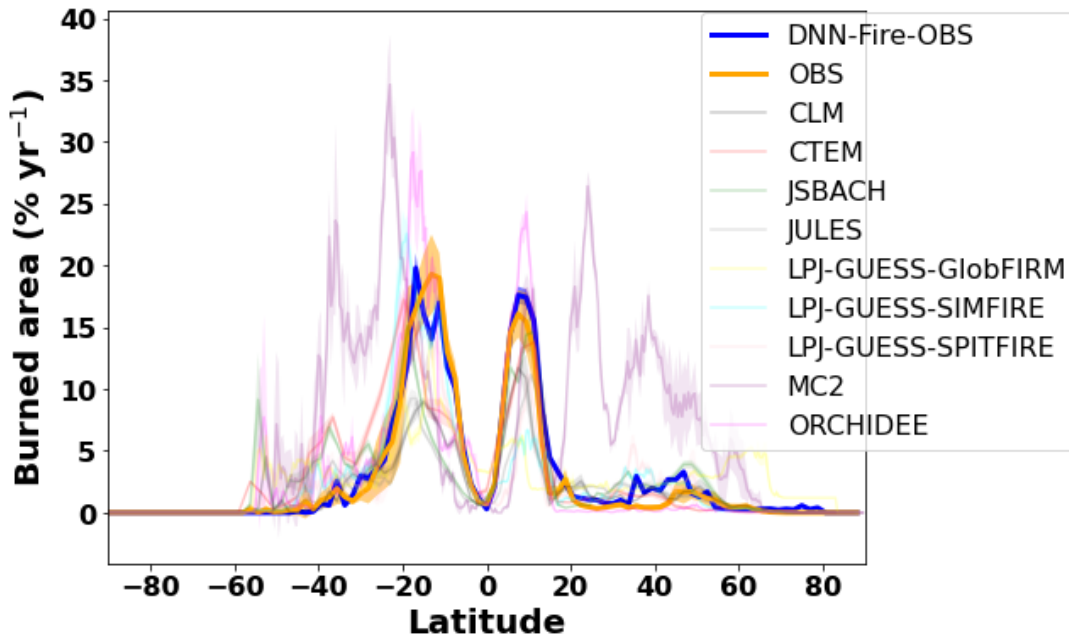
323 We next evaluated the DNN-Fire-OBS model against observations for the period 2011 to
 324 2015, using data which were not used to train and validate the model. Overall, DNN-Fire-OBS

325 simulated 469-514 Mha yr⁻¹ global burned area, compared with observations 349-509 Mha yr⁻¹.
 326 Note that the large observational ranges were mainly due to the differences among the five
 327 burned area products rather than the inter-annual variability (Figure 6). Regionally, DNN-Fire-
 328 OBS overestimated NHAF, SHAF and SHSA annual burned area by 8, 6, 2 Mha yr⁻¹,
 329 respectively (Figure 6) compared with the observational mean. Averaged latitudinal distribution
 330 of simulated burned area during this period showed that global wildfire activity peaked around
 331 S10°- S15° and N5°-N10°, together accounting for burning 12-16% of the land surface (Figure
 332 7). These two peaks were dominated by large burned area over Southern (SHAF) and Northern
 333 Hemisphere Africa (NHAF) fire regions. Compared with observations, DNN-Fire-OBS
 334 simulated reasonable burned area latitudinal distributions (Figure 7). We also compared the nine
 335 FireMIP models [Rabin *et al.*, 2017; Teckentrup *et al.*, 2018] and found diverse latitudinal
 336 distribution of burned area. The across model differences were much larger than the inter-annual
 337 variation simulated by each individual model, which indicated large model structural
 338 uncertainties. Validation was also conducted for the historical period 1981-2000, when most of
 339 the satellite based burned area data were not available. Compared with charcoal index inferred
 340 burned area during 1981-2000 (Figure S4), DNN-Fire-OBS model reasonably captured the
 341 declining of burned area from ~530 Mha yr⁻¹ to 490 Mha yr⁻¹. In summary, DNN-Fire-OBS
 342 simulation is reasonably accurate and: (1) improved the simulated wildfire spatial and temporal
 343 distributions in ELMv1; (2) enabled effective and efficient parameterization of fires at regional
 344 scale.
 345



346

347 **Figure 6.** Prognostic simulation of annual wildfire burned area with the Deep Neural Network
348 wildfire model fine-tuned with observations (DNN-Fire-OBS) compared with five burned area
349 products (Table S1) over 2011-2015 for 14 GFED regions.
350



351
352 **Figure 7.** Prognostic simulation of wildfire burned area (2011-2015) with the Deep Neural
353 Network wildfire model fine-tuned with observations (DNN-Fire-OBS) compared with
354 observations and nine FireMIP models outputs.
355

356 This study focuses on design, development, and parameterization of the DNN fire model
357 within the E3SM model interface. In this way the DNN model can be readily coupled in the
358 future and iteratively simulate climate, ecosystem fuel conditions, and fire dynamics. This study
359 is an important step towards fully coupling E3SM and the DNN-Fire models in the future. We
360 acknowledge several challenges and limitations in our modeling framework. First, the DNN
361 model uncertainty was subject to the accuracy of climate forcings as well as other physical
362 driving variables simulated by the physical wildfire model (ELMv1). For example, in addition to
363 the default GSWP3 climate forcings dataset used in the study, CRU-JRA [Onogi *et al.*, 2007]
364 and NCEP-DOE2 [Kanamitsu *et al.*, 2002] reanalysis forcings were also widely used and
365 potentially different from GSWP3 forcings. ELMv1 used climate forcing (*e.g.*, temperature,
366 precipitation, wind speed, relative humidity) to simulate soil temperature, soil moisture, fuel load

367 and so on. These simulated variables served as inputs for the DNN model and could also result in
368 prediction uncertainty. It was challenging to eliminate the forcing uncertainties in this work, but
369 we could at least evaluate the magnitude of these uncertainties. We ran the DNN-Fire-OBS
370 model with alternative forcings of CRU-JRA, NCEP-DOE2, and CDAS soil moisture from 2001
371 to 2010 and compared the results with DNN-Fire-OBS driven by default inputs (GSWP3 climate
372 and ELMv1 simulated soil moisture) (Figure S5). The results showed relatively larger
373 uncertainties from climate forcing than that from soil moisture forcing particularly over the
374 major fire regions (e.g., SHSA, SHAF, and NHAF). For fuel load, although no transient dataset
375 of global living biomass existed yet, we directly compared the ELM model simulated biomass
376 with the global estimate (GEOCARBON ~ 455 Pg C). We found that the modeled present-day
377 biomass continuously increased from 425 to 470 Pg C and compared reasonably well with the
378 global benchmark (Figure S6). Future work will focus on evaluating the uncertainties from dead
379 fuel load and fuel temperature variables.

380 Second, the original ELMv1 wildfire model has a unified mathematical representation of
381 how fuel, climate, and social-economic conditions control wildfire burned area [*F Li et al.*,
382 2012]. However, training one single DNN wildfire model across the globe will produce a model
383 dominated by gridcells that have high burned area (e.g., Africa). The performance of the trained
384 DNN model, therefore, will likely have larger biases over the low fire gridcells although the
385 globally aggregated burned area could be reasonable. We partly overcame this challenge by
386 applying the widely used 14 GFED fire regions that assume unique and relatively uniform
387 dynamics over each region [*Giglio et al.*, 2006b], and employed stratified random sampling
388 method for training and testing datasets. Although the regionally specific wildfire model
389 introduces additional complexity, it better represents distinct characteristics of wildfire activity
390 over different climate regimes and biomes [*Zhu and Zhuang*, 2013; *Zou et al.*, 2019] and allows
391 for future analyses of how the relevant controllers vary across the globe.

392 Finally, our GFED region-based parameterization strategy relied on the combination of
393 climate and biome types, while an alternative parameterization strategy for DNN-Fire model
394 could be based on plant functional type distributions. Based on our analysis, the PFT-based
395 DNN-Fire model had similar performance compared with the GFED-based model (Figure S7,
396 S8). Since the current version of the E3SM land model does not allow PFT changes driven by

397 climate, both GFED-based and PFT-based models may not fully capture the changes of fire
398 dynamics due to longer-time scale fire regimes changes.

399

400 **4. Conclusions**

401 In this study, we first surrogated the baseline ELMv1 wildfire model with a Deep Neural
402 Network (DNN) approach (Pearson correlation coefficient = 0.91 (p value < 0.01), $R^2 = 0.79$).
403 The development was based on inputs and outputs from the baseline ELMv1 wildfire simulation,
404 which is process-based and reasonably simulates global burned area, although regional biases
405 existed. We then calibrated the neural network weights using the years 2001-2010
406 observationally inferred burned area. The final calibrated DNN wildfire model (DNN-Fire-OBS)
407 was shown to be more accurate over the 14 GFED regions. For example, reductions in absolute
408 error over Africa, South America, and Europe were by ~90%. More importantly, the DNN-Fire-
409 OBS model parameters could be calibrated within minutes, compared with traditional ELMv1
410 parameterization ensemble simulations that consume a large amount of computational time. The
411 improved DNN-Fire-OBS model also accurately prognosed global and regional burned area in
412 the five-year period following the training period from 2011 to 2015 (modeled 469-514 Mha yr⁻¹).
413 We conclude that the improved surrogate wildfire model (DNN-Fire-OBS) developed in this
414 study can serve as an effective alternative to the process-based fire model currently used in
415 ELMv1. More broadly, we conclude that machine learning techniques can facilitate earth system
416 model development, parameterization, and uncertainty reduction with high efficiency and
417 accuracy.

418

419 **Acknowledgements**

420 This research was supported by Energy Exascale Earth System Modeling (E3SM,
421 <https://e3sm.org/>) Project and the Reducing Uncertainties in Biogeochemical Interactions
422 through Synthesis and Computation (RUBISCO) Scientific Focus Area, Office of Biological and
423 Environmental Research of the U.S. Department of Energy Office of Science. Lawrence
424 Berkeley National Laboratory (LBNL) is managed by the University of California for the U.S.
425 Department of Energy under contract DE-AC02-05CH11231.

426

427 **Author contribution**

428 Q.Z., W.J.R, designed the study, Q.Z., W.J.R, L.X., and J.T.R designed model experiments,
429 Q.Z. and F.L. wrote code and run experiments, L.Z, K.Y, H.W., J.G all contribute to the results
430 interpretation, and writing.

431

432 **Code availability**

433 https://github.com/qzhu-lbl/ANN_wildfire

434 **Data availability**

435 **GFEDv4s:** https://daac.ornl.gov/VEGETATION/guides/fire_emissions_v4.html

436 **Fire_CCI51:** https://geogra.uah.es/fire_cci/firecci51.php

437 **Fire_CCILT11:** https://geogra.uah.es/fire_cci/fireccilt11.php

438 **MCD64:** https://modis-fire.umd.edu/files/MODIS_C6_Fire_User_Guide_C.pdf

439 **Fire Atlas:** <https://www.globalfiredata.org/fireatlas.html>

440 **FireMIP model outputs:** <https://zenodo.org/record/3555562/accessrequest>

441

442 **Reference**

443 Abatzoglou, J. T., and A. P. Williams (2016), Impact of anthropogenic climate change on wildfire
444 across western US forests, *Proceedings of the National Academy of Sciences*, *113*(42),
445 11770-11775.

446 Andela, N., D. Morton, L. Giglio, Y. Chen, G. Van Der Werf, P. Kasibhatla, R. DeFries, G. Collatz, S.
447 Hantson, and S. Kloster (2017), A human-driven decline in global burned area, *Science*,
448 *356*(6345), 1356-1362.

449 Andela, N., D. C. Morton, L. Giglio, R. Paugam, Y. Chen, S. Hantson, G. R. Van Der Werf, and J. T.
450 Randerson (2019), The Global Fire Atlas of individual fire size, duration, speed and
451 direction, *Earth System Science Data*, *11*(2), 529-552.

452 Arora, V. K., and G. J. Boer (2005), Fire as an interactive component of dynamic vegetation
453 models, *Journal of Geophysical Research: Biogeosciences*, *110*(G2).

454 Bond, W. J., F. I. Woodward, and G. F. Midgley (2005), The global distribution of ecosystems in a
455 world without fire, *New phytologist*, *165*(2), 525-538.

456 Bond-Lamberty, B., S. D. Peckham, D. E. Ahl, and S. T. Gower (2007), Fire as the dominant driver
457 of central Canadian boreal forest carbon balance, *Nature*, *450*(7166), 89-92.

458 Bowd, E. J., S. C. Banks, C. L. Strong, and D. B. Lindenmayer (2019), Long-term impacts of
459 wildfire and logging on forest soils, *Nature Geoscience*, *12*(2), 113-118.

460 Brando, P., B. Soares-Filho, L. Rodrigues, A. Assunção, D. Morton, D. Tuchsneider, E.
461 Fernandes, M. Macedo, U. Oliveira, and M. Coe (2020), The gathering firestorm in
462 southern Amazonia, *Science advances*, *6*(2), eaay1632.

463 Cecil, D. J., D. E. Buechler, and R. J. Blakeslee (2014), Gridded lightning climatology from TRMM-
464 LIS and OTD: Dataset description, *Atmospheric Research*, *135*, 404-414.

465 Chambers, S., and F. Chapin (2002), Fire effects on surface-atmosphere energy exchange in
466 Alaskan black spruce ecosystems: Implications for feedbacks to regional climate, *Journal*
467 *of Geophysical Research: Atmospheres*, 107(D1), FFR 1-1-FFR 1-17.

468 Chen, Y., J. T. Randerson, S. R. Coffield, E. Foufoula-Georgiou, P. Smyth, C. A. Graff, D. C.
469 Morton, N. Andela, G. R. van der Werf, and L. Giglio (2020), Forecasting global fire
470 emissions on subseasonal to seasonal (S2S) time scales, *Journal of advances in modeling*
471 *earth systems*, 12(9), e2019MS001955.

472 Chen, Y., J. T. Randerson, D. C. Morton, R. S. DeFries, G. J. Collatz, P. S. Kasibhatla, L. Giglio, Y.
473 Jin, and M. E. Marlier (2011), Forecasting fire season severity in South America using sea
474 surface temperature anomalies, *Science*, 334(6057), 787-791.

475 Clark, T. L., J. Coen, and D. Latham (2004), Description of a coupled atmosphere–fire model,
476 *International Journal of Wildland Fire*, 13(1), 49-63.

477 Coffield, S. R., C. A. Graff, Y. Chen, P. Smyth, E. Foufoula-Georgiou, and J. T. Randerson (2019),
478 Machine learning to predict final fire size at the time of ignition, *International journal of*
479 *wildland fire*.

480 Day, C. (2004), Smoke from burning vegetation changes the coverage and behavior of clouds,
481 *PhT*, 57(5), 24-24.

482 Dirmeyer, P. A., X. Gao, M. Zhao, Z. Guo, T. Oki, and N. Hanasaki (2006), GSWP-2: Multimodel
483 analysis and implications for our perception of the land surface, *Bulletin of the American*
484 *Meteorological Society*, 87(10), 1381-1398.

485 Dobson, J. E., E. A. Bright, P. R. Coleman, R. C. Durfee, and B. A. Worley (2000), LandScan: a
486 global population database for estimating populations at risk, *Photogrammetric*
487 *engineering and remote sensing*, 66(7), 849-857.

488 Finney, M. A. (1998), *FARSITE, Fire Area Simulator--model development and evaluation*, US
489 Department of Agriculture, Forest Service, Rocky Mountain Research Station.

490 French, N. H., M. A. Whitley, and L. K. Jenkins (2016), Fire disturbance effects on land surface
491 albedo in Alaskan tundra, *Journal of Geophysical Research: Biogeosciences*, 121(3), 841-
492 854.

493 Ganapathi Subramanian, S., and M. Crowley (2018), Using spatial reinforcement learning to
494 build forest wildfire dynamics models from satellite images, *Frontiers in ICT*, 5, 6.

495 Giglio, L., L. Boschetti, D. P. Roy, M. L. Humber, and C. O. Justice (2018), The Collection 6 MODIS
496 burned area mapping algorithm and product, *Remote sensing of environment*, 217, 72-
497 85.

498 Giglio, L., I. Csiszar, and C. O. Justice (2006a), Global distribution and seasonality of active fires
499 as observed with the Terra and Aqua Moderate Resolution Imaging Spectroradiometer
500 (MODIS) sensors, *Journal of geophysical research: Biogeosciences*, 111(G2).

501 Giglio, L., J. T. Randerson, and G. R. Van Der Werf (2013), Analysis of daily, monthly, and annual
502 burned area using the fourth-generation global fire emissions database (GFED4), *Journal*
503 *of Geophysical Research: Biogeosciences*, 118(1), 317-328.

504 Giglio, L., G. Van der Werf, J. Randerson, G. Collatz, and P. Kasibhatla (2006b), Global estimation
505 of burned area using MODIS active fire observations.

506 Girardin, M. P., and M. Mudelsee (2008), Past and future changes in Canadian boreal wildfire
507 activity, *Ecological Applications*, 18(2), 391-406.

508 Goodfellow, I., Y. Bengio, and A. Courville (2016), *Deep learning*, MIT press Cambridge.

509 Goss, M., D. L. Swain, J. T. Abatzoglou, A. Sarhadi, C. A. Kolden, A. P. Williams, and N. S.
510 Diffenbaugh (2020), Climate change is increasing the likelihood of extreme autumn
511 wildfire conditions across California, *Environmental Research Letters*, 15(9), 094016.
512 Harden, J. W., K. L. Manies, M. R. Turetsky, and J. C. Neff (2006), Effects of wildfire and
513 permafrost on soil organic matter and soil climate in interior Alaska, *Global Change*
514 *Biology*, 12(12), 2391-2403.
515 Heyerdahl, E. K., L. B. Brubaker, and J. K. Agee (2002), Annual and decadal climate forcing of
516 historical fire regimes in the interior Pacific Northwest, USA, *The Holocene*, 12(5), 597-
517 604.
518 Holden, Z. A., A. Swanson, C. H. Luce, W. M. Jolly, M. Maneta, J. W. Oyler, D. A. Warren, R.
519 Parsons, and D. Affleck (2018), Decreasing fire season precipitation increased recent
520 western US forest wildfire activity, *Proceedings of the National Academy of Sciences*,
521 115(36), E8349-E8357.
522 Hurtt, G. C., L. Chini, R. Sahajpal, S. Frohling, B. L. Boudirsky, K. Calvin, J. C. Doelman, J. Fisk, S.
523 Fujimori, and K. K. Goldewijk (2020), Harmonization of global land-use change and
524 management for the period 850–2100 (LUH2) for CMIP6, *Geoscientific Model*
525 *Development Discussions*, 1-65.
526 Jiang, Y., X.-Q. Yang, X. Liu, Y. Qian, K. Zhang, M. Wang, F. Li, Y. Wang, and Z. Lu (2020), Impacts
527 of wildfire aerosols on global energy budget and climate: The role of climate feedbacks,
528 *Journal of Climate*, 33(8), 3351-3366.
529 Kanamitsu, M., W. Ebisuzaki, J. Woollen, S.-K. Yang, J. Hnilo, M. Fiorino, and G. Potter (2002),
530 Ncep–doe amip-ii reanalysis (r-2), *Bulletin of the American Meteorological Society*,
531 83(11), 1631-1644.
532 Kasischke, E. S., and L. P. Bruhwiler (2002), Emissions of carbon dioxide, carbon monoxide, and
533 methane from boreal forest fires in 1998, *Journal of Geophysical Research:*
534 *Atmospheres*, 107(D1), FFR 2-1-FFR 2-14.
535 Keeley, J. E., and A. D. Syphard (2018), Historical patterns of wildfire ignition sources in
536 California ecosystems, *International journal of wildland fire*, 27(12), 781-799.
537 Kelley, D. I., I. Bistinas, R. Whitley, C. Burton, T. R. Marthews, and N. Dong (2019), How
538 contemporary bioclimatic and human controls change global fire regimes, *Nature*
539 *Climate Change*, 9(9), 690-696.
540 Kingma, D. P., and J. Ba (2014), Adam: A method for stochastic optimization, *arXiv preprint*
541 *arXiv:1412.6980*.
542 Knorr, W., T. Kaminski, A. Arneth, and U. Weber (2014), Impact of human population density on
543 fire frequency at the global scale, *Biogeosciences*, 11(4), 1085-1102.
544 Koven, C. D., W. J. Riley, Z. M. Subin, J. Y. Tang, M. S. Torn, W. D. Collins, G. B. Bonan, D. M.
545 Lawrence, and S. C. Swenson (2013), The effect of vertically resolved soil
546 biogeochemistry and alternate soil C and N models on C dynamics of CLM4,
547 *Biogeosciences*, 10, 7109-7131.
548 Lamarque, J. F., J. T. Kiehl, G. P. Brasseur, T. Butler, P. Cameron-Smith, W. D. Collins, W. J.
549 Collins, C. Granier, D. Hauglustaine, and P. G. Hess (2005), Assessing future nitrogen
550 deposition and carbon cycle feedback using a multimodel approach: Analysis of nitrogen
551 deposition, *Journal of Geophysical Research: Atmospheres*, 110(D19).

552 Lasslop, G., S. Hantson, S. P. Harrison, D. Bachelet, C. Burton, M. Forkel, M. Forrest, F. Li, J. R.
553 Melton, and C. Yue (2020), Global ecosystems and fire: Multi-model assessment of fire-
554 induced tree-cover and carbon storage reduction, *Global change biology*, 26(9), 5027-
555 5041.

556 Lenihan, J. M., and D. Bachelet (2015), Historical climate and suppression effects on simulated
557 fire and carbon dynamics in the conterminous United States, *Global Vegetation*
558 *Dynamics: Concepts and Applications in the MC1 Model*, edited by: Bachelet, D. and
559 Turner, D., *AGU Geophysical Monographs*, 214, 17-30.

560 Li, F., M. Val Martin, M. O. Andreae, A. Arneth, S. Hantson, J. W. Kaiser, G. Lasslop, C. Yue, D.
561 Bachelet, and M. Forrest (2019), Historical (1700–2012) global multi-model estimates of
562 the fire emissions from the Fire Modeling Intercomparison Project (FireMIP),
563 *Atmospheric Chemistry and Physics*, 19(19), 12545-12567.

564 Li, F., X. Zeng, and S. Levis (2012), A process-based fire parameterization of intermediate
565 complexity in a Dynamic Global Vegetation Model, *Biogeosciences*, 9(7).

566 Lizundia-Loiola, J., G. Otón, R. Ramo, and E. Chuvieco (2020), A spatio-temporal active-fire
567 clustering approach for global burned area mapping at 250 m from MODIS data, *Remote*
568 *Sensing of Environment*, 236, 111493.

569 Lizundia-Loiola, J., M. Pettinari, E. Chuvieco, T. Storm, and J. Gómez-Dans (2018), ESA CCI ECV
570 Fire Disturbance: Algorithm Theoretical Basis Document-MODIS, version 2.0, edited,
571 Fire_cci_D2.

572 Mahowald, N., T. D. Jickells, A. R. Baker, P. Artaxo, C. R. Benitez-Nelson, G. Bergametti, T. C.
573 Bond, Y. Chen, D. D. Cohen, and B. Herut (2008), Global distribution of atmospheric
574 phosphorus sources, concentrations and deposition rates, and anthropogenic impacts,
575 *Global Biogeochemical Cycles*, 22(4).

576 Mekonnen, Z. A., W. J. Riley, J. T. Randerson, R. F. Grant, and B. M. Rogers (2019), Expansion of
577 high-latitude deciduous forests driven by interactions between climate warming and
578 fire, *Nature plants*, 5(9), 952-958.

579 Oliver, A. K., M. A. Callaham Jr, and A. Jumpponen (2015), Soil fungal communities respond
580 compositionally to recurring frequent prescribed burning in a managed southeastern US
581 forest ecosystem, *Forest Ecology and Management*, 345, 1-9.

582 Onogi, K., J. Tsutsui, H. Koide, M. Sakamoto, S. Kobayashi, H. Hatsushika, T. Matsumoto, N.
583 Yamazaki, H. Kamahori, and K. Takahashi (2007), The JRA-25 reanalysis, *Journal of the*
584 *Meteorological Society of Japan. Ser. II*, 85(3), 369-432.

585 Papakosta, P., G. Xanthopoulos, and D. Straub (2017), Probabilistic prediction of wildfire
586 economic losses to housing in Cyprus using Bayesian network analysis, *International*
587 *journal of wildland fire*, 26(1), 10-23.

588 Pellegrini, A. F., A. Ahlström, S. E. Hobbie, P. B. Reich, L. P. Nieradzic, A. C. Staver, B. C.
589 Scharenbroch, A. Jumpponen, W. R. Anderegg, and J. T. Randerson (2018), Fire
590 frequency drives decadal changes in soil carbon and nitrogen and ecosystem
591 productivity, *Nature*, 553(7687), 194-198.

592 Pellegrini, A. F., S. E. Hobbie, P. B. Reich, A. Jumpponen, E. J. Brookshire, A. C. Caprio, C.
593 Coetsee, and R. B. Jackson (2020), Repeated fire shifts carbon and nitrogen cycling by
594 changing plant inputs and soil decomposition across ecosystems, *Ecological*
595 *Monographs*, e01409.

596 Preisler, H. K., and A. L. Westerling (2007), Statistical model for forecasting monthly large
597 wildfire events in western United States, *Journal of Applied Meteorology and*
598 *Climatology*, 46(7), 1020-1030.

599 Prentice, S., and D. Mackerras (1977), The ratio of cloud to cloud-ground lightning flashes in
600 thunderstorms, *Journal of Applied Meteorology*, 16(5), 545-550.

601 Rabin, S. S., J. R. Melton, G. Lasslop, D. Bachelet, M. Forrest, S. Hantson, J. O. Kaplan, F. Li, S.
602 Mangeon, and D. S. Ward (2017), The Fire Modeling Intercomparison Project (FireMIP),
603 phase 1: experimental and analytical protocols with detailed model descriptions,
604 *Geoscientific Model Development*, 10(3), 1175-1197.

605 Radke, D., A. Hessler, and D. Ellsworth (2019), FireCast: Leveraging Deep Learning to Predict
606 Wildfire Spread, paper presented at IJCAI.

607 Randerson, J. T., H. Liu, M. G. Flanner, S. D. Chambers, Y. Jin, P. G. Hess, G. Pfister, M. Mack, K.
608 Treseder, and L. Welp (2006), The impact of boreal forest fire on climate warming,
609 *science*, 314(5802), 1130-1132.

610 Riley, K., and M. Thompson (2017), An uncertainty analysis of wildfire modeling, *Natural hazard*
611 *uncertainty assessment: modeling and decision support. Monograph*, 223, 193-213.

612 Ross, A. N., M. J. Wooster, H. Boesch, and R. Parker (2013), First satellite measurements of
613 carbon dioxide and methane emission ratios in wildfire plumes, *Geophysical Research*
614 *Letters*, 40(15), 4098-4102.

615 Rother, D., and F. De Sales (2020), Impact of Wildfire on the Surface Energy Balance in Six
616 California Case Studies, *Boundary-Layer Meteorology*, 1-24.

617 Saha, M. V., T. M. Scanlon, and P. D'Odorico (2019), Climate seasonality as an essential
618 predictor of global fire activity, *Global Ecology and Biogeography*, 28(2), 198-210.

619 Sayad, Y. O., H. Mousannif, and H. Al Moatassime (2019), Predictive modeling of wildfires: A
620 new dataset and machine learning approach, *Fire safety journal*, 104, 130-146.

621 Schmidhuber, J. (2015), Deep learning in neural networks: An overview, *Neural networks*, 61,
622 85-117.

623 Stephenson, C., J. Handmer, and R. Betts (2013), Estimating the economic, social and
624 environmental impacts of wildfires in Australia, *Environmental Hazards*, 12(2), 93-111.

625 Syphard, A. D., V. C. Radeloff, J. E. Keeley, T. J. Hawbaker, M. K. Clayton, S. I. Stewart, and R. B.
626 Hammer (2007), Human influence on California fire regimes, *Ecological applications*,
627 17(5), 1388-1402.

628 Teckentrup, L., G. Lasslop, D. Bachelet, M. Forrest, S. Hantson, F. Li, J. R. Melton, C. Yue, A.
629 Arneth, and S. P. Harrison (2018), Simulations of historical burned area: A comparison of
630 global fire models in FireMIP, *EGUGA*, 17537.

631 Thonicke, K., A. Spessa, I. Prentice, S. P. Harrison, L. Dong, and C. Carmona-Moreno (2010), The
632 influence of vegetation, fire spread and fire behaviour on biomass burning and trace gas
633 emissions: results from a process-based model, *Biogeosciences*, 7(6), 1991-2011.

634 Tonini, M., M. D'Andrea, G. Biondi, S. Degli Esposti, A. Trucchia, and P. Fiorucci (2020), A
635 Machine Learning-Based Approach for Wildfire Susceptibility Mapping. The Case Study
636 of the Liguria Region in Italy, *Geosciences*, 10(3), 105.

637 Van Der Werf, G. R., J. T. Randerson, L. Giglio, T. T. Van Leeuwen, Y. Chen, B. M. Rogers, M. Mu,
638 M. J. Van Marle, D. C. Morton, and G. J. Collatz (2017), Global fire emissions estimates
639 during 1997-2016, *Earth System Science Data*, 9(2), 697-720.

640 van Vuuren, D. P., P. L. Lucas, and H. Hilderink (2007), Downscaling drivers of global
641 environmental change: Enabling use of global SRES scenarios at the national and grid
642 levels, *Global environmental change*, 17(1), 114-130.

643 Venevsky, S., K. Thonicke, S. Sitch, and W. Cramer (2002), Simulating fire regimes in human-
644 dominated ecosystems: Iberian Peninsula case study, *Global Change Biology*, 8(10), 984-
645 998.

646 Walker, X. J., J. L. Baltzer, S. G. Cumming, N. J. Day, C. Ebert, S. Goetz, J. F. Johnstone, S. Potter,
647 B. M. Rogers, and E. A. Schuur (2019), Increasing wildfires threaten historic carbon sink
648 of boreal forest soils, *Nature*, 572(7770), 520-523.

649 Wang, J.-F., A. Stein, B.-B. Gao, and Y. Ge (2012), A review of spatial sampling, *Spatial Statistics*,
650 2, 1-14.

651 Westerling, A. L., H. G. Hidalgo, D. R. Cayan, and T. W. Swetnam (2006), Warming and earlier
652 spring increase western US forest wildfire activity, *science*, 313(5789), 940-943.

653 Williams, A. P., J. T. Abatzoglou, A. Gershunov, J. Guzman-Morales, D. A. Bishop, J. K. Balch, and
654 D. P. Lettenmaier (2019), Observed impacts of anthropogenic climate change on wildfire
655 in California, *Earth's Future*, 7(8), 892-910.

656 Xu, X., G. Jia, X. Zhang, W. J. Riley, and Y. Xue (2020), Climate regime shift and forest loss
657 amplify fire in Amazonian forests, *Global Change Biology*, 26(10), 5874-5885.

658 Yu, Y., J. Mao, P. E. Thornton, M. Notaro, S. D. Wullschleger, X. Shi, F. M. Hoffman, and Y. Wang
659 (2020), Quantifying the drivers and predictability of seasonal changes in African fire,
660 *Nature Communications*, 11(1), 1-8.

661 Yue, X., L. J. Mickley, J. A. Logan, and J. O. Kaplan (2013), Ensemble projections of wildfire
662 activity and carbonaceous aerosol concentrations over the western United States in the
663 mid-21st century, *Atmospheric Environment*, 77, 767-780.

664 Zheng, H., Z. Yang, W. Liu, J. Liang, and Y. Li (2015), Improving deep neural networks using
665 softplus units, paper presented at 2015 International Joint Conference on Neural
666 Networks (IJCNN), IEEE.

667 Zhu, Q., and W. J. Riley (2015), Improved modelling of soil nitrogen losses, *Nature Climate
668 Change*, 5(8), 705-706.

669 Zhu, Q., W. J. Riley, C. M. Iversen, and J. Kattge (2020), Assessing impacts of plant stoichiometric
670 traits on terrestrial ecosystem carbon accumulation using the E3SM land model, *Journal
671 of Advances in Modeling Earth Systems*, 12(4), e2019MS001841.

672 Zhu, Q., W. J. Riley, J. Tang, N. Collier, F. M. Hoffman, X. Yang, and G. Bisht (2019), Representing
673 nitrogen, phosphorus, and carbon interactions in the E3SM Land Model: Development
674 and global benchmarking, *Journal of Advances in Modeling Earth Systems*, doi:
675 10.1029/2018MS001571.

676 Zhu, Q., W. J. Riley, J. Tang, and C. D. Koven (2016), Multiple soil nutrient competition between
677 plants, microbes, and mineral surfaces: model development, parameterization, and
678 example applications in several tropical forests, *Biogeosciences*, 13, 341-363,
679 doi:10.5194/bgd-12-4057-2015.

680 Zhu, Q., and Q. Zhuang (2013), Improving the quantification of terrestrial ecosystem carbon
681 dynamics over the United States using an adjoint method, *Ecosphere*, 4(10), doi:
682 dx.doi.org/10.1890/ES1813-00058.00051.

683 Zhu, Q., and Q. Zhuang (2014), Parameterization and sensitivity analysis of a process-based
684 terrestrial ecosystem model using adjoint method, *Journal of Advances in Modeling*
685 *Earth Systems*, 6(2), 315-331.

686 Zou, Y., Y. Wang, Z. Ke, H. Tian, J. Yang, and Y. Liu (2019), Development of a REgion-specific
687 ecosystem feedback fire (RESFire) model in the Community Earth System Model, *Journal*
688 *of Advances in Modeling Earth Systems*, 11(2), 417-445.

689 Zou, Y., Y. Wang, Y. Qian, H. Tian, J. Yang, and E. Alvarado (2020), Using CESM-RESFire to
690 understand climate-fire-ecosystem interactions and the implications for decadal climate
691 variability, *Atmospheric Chemistry and Physics*, 20(PNNL-SA-150222).

692

693 **Supplementary Material**

694

695 Table S1. Burned area datasets used in this study

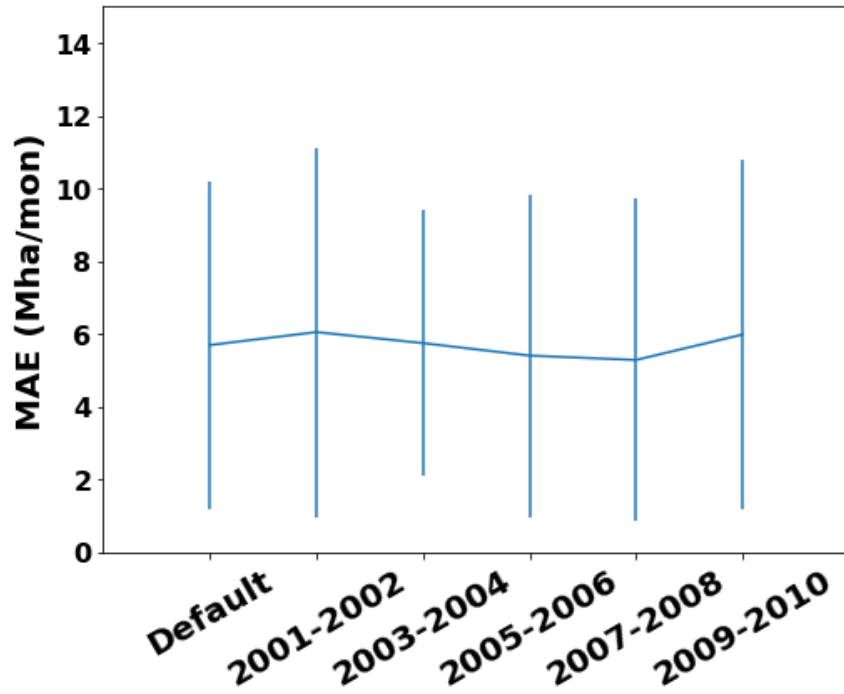
696

Dataset name	Temporal range	Spatial resolution	Burned area, mean (std)	Citations
GFEDv4s	1997-2015	0.25 degree	455(39)	(Van Der Werf, Randerson et al. 2017)
Fire_CCI51	2001-2019	0.25 degree	476(26)	(Lizundia-Loiola, Otón et al. 2020)
Fire_CCILT11	1982-2018	0.25 degree	484(20)	(Lizundia-Loiola, Pettinari et al. 2018)
MCD64	2001-2019	0.25 degree	424(35)	(Giglio, Boschetti et al. 2018)
Fire_Atlas	2003-2016	0.25x0.25 degree	459(43)	(Andela, Morton et al. 2019)

697 **Note:** the long-term average global burned area was calculated using data with the same698 overlapping temporal range (2003-2015), unit Mha yr⁻¹

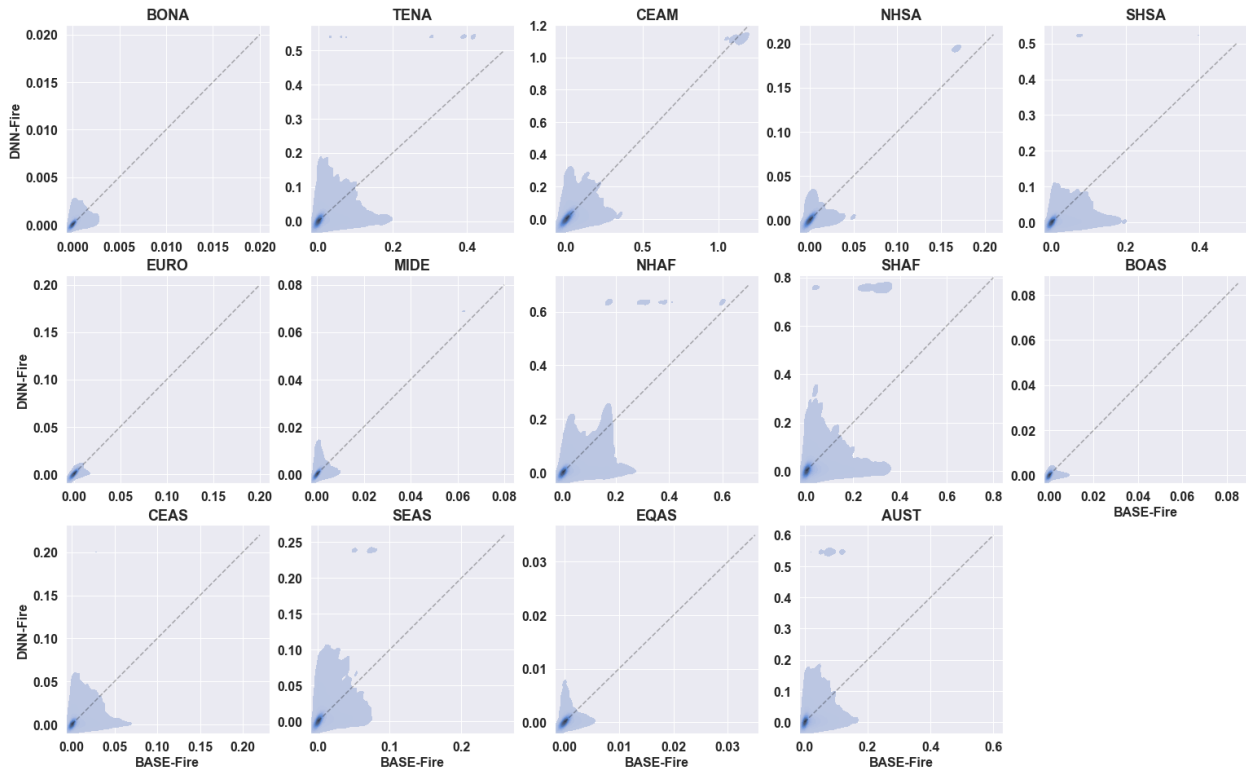
699

700



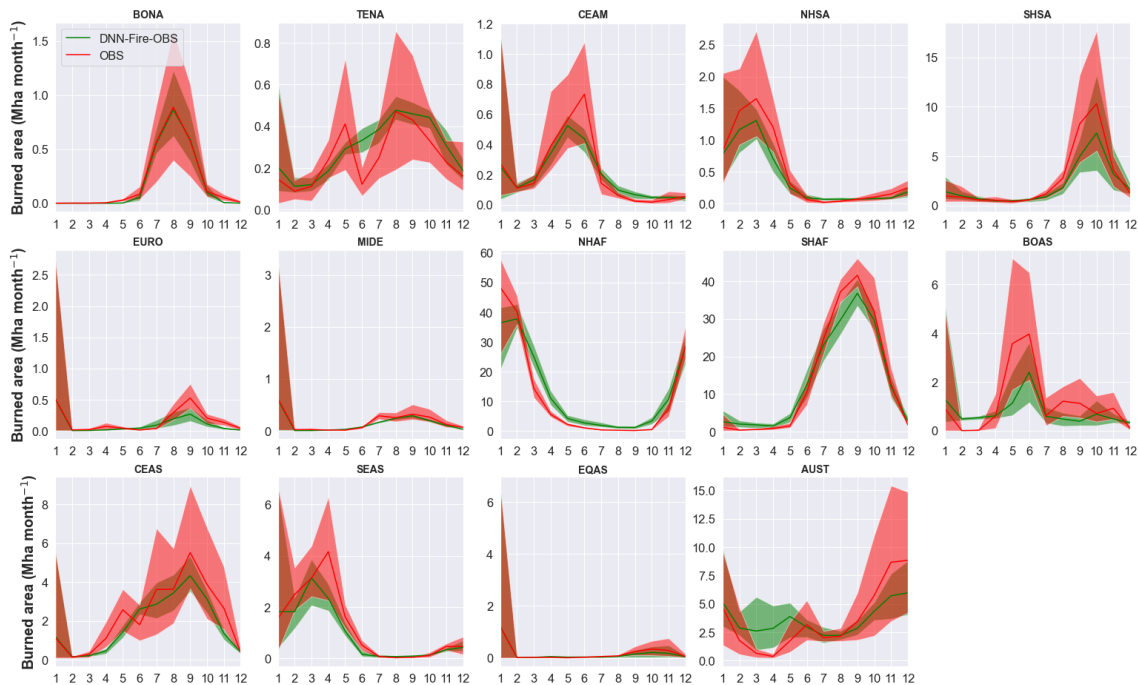
701
702
703
704
705

Figure S1. Model performance evaluated with testing datasets of default (20% randomly selected samples), or fixed to 2001-2002 period, 2003-2004 period, 2005-2006 period, 2007-2008 period, and 2009-2010 periods (the rest of the dataset was used as a training dataset.).

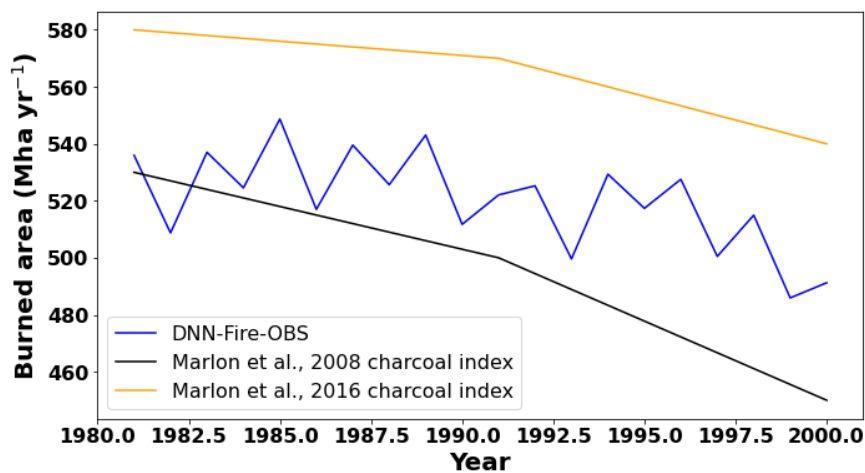


706

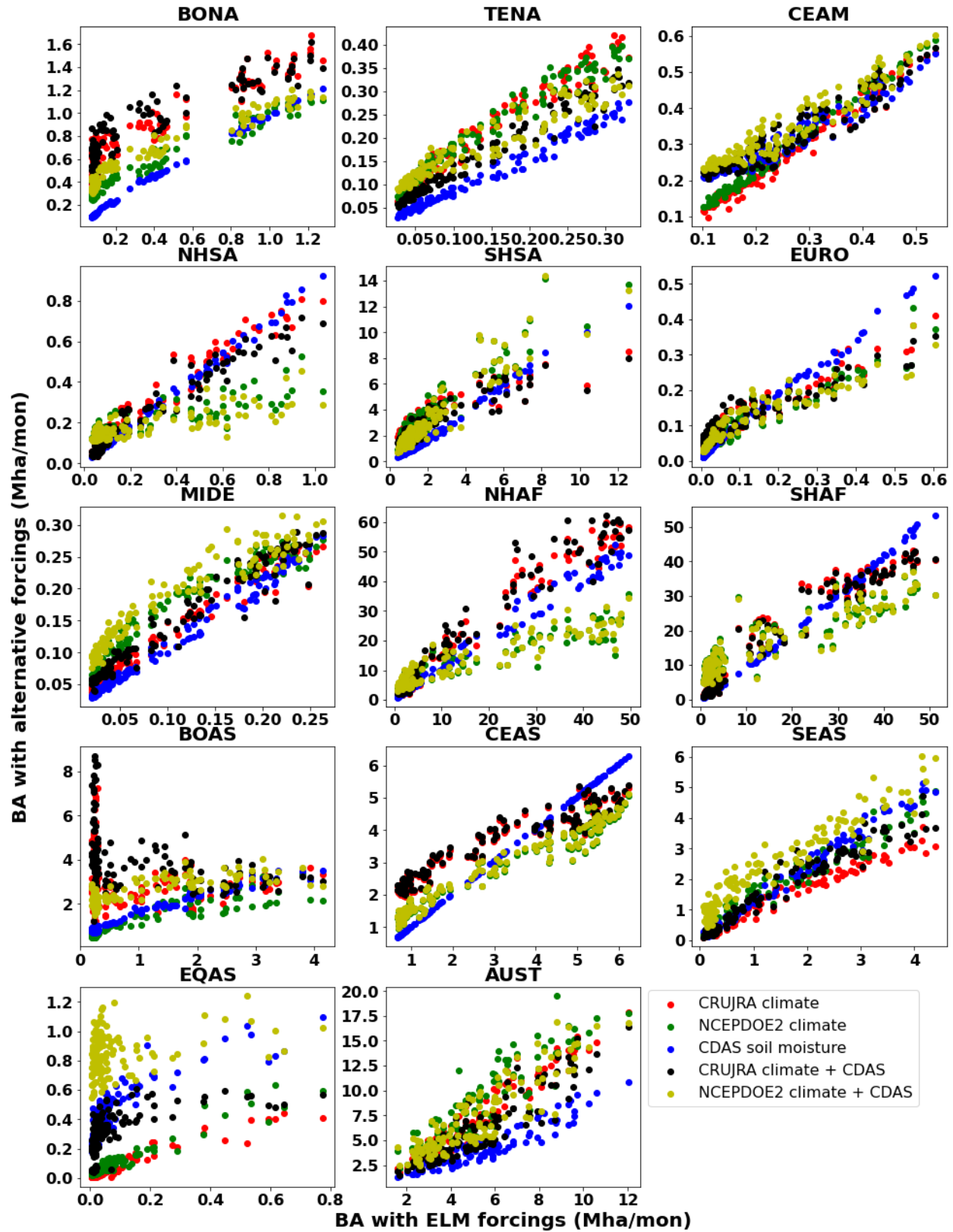
707 **Figure S2.** Performance of surrogate model (DNN-Fire) compared with ELMv1 process-based
 708 model (BASE-Fire).
 709



710 **Figure S3.** Seasonal cycles of fine-tuned Deep Neural Network wildfire model (DNN-Fire-OBS)
 711 and observations over 14 GFED fire regions.
 712
 713
 714



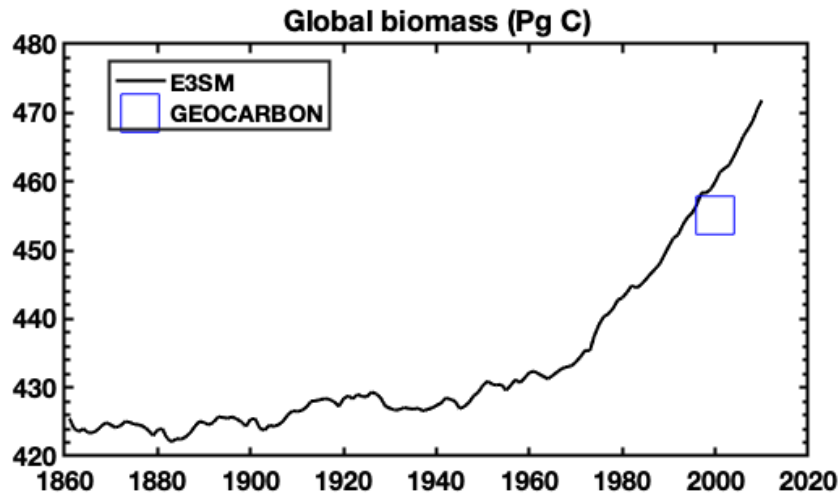
715 **Figure S4.** Comparison of DNN-Fire-OBS model simulated global burned area during 1981-
 716 1999 with two charcoal index inferred burned area.
 717



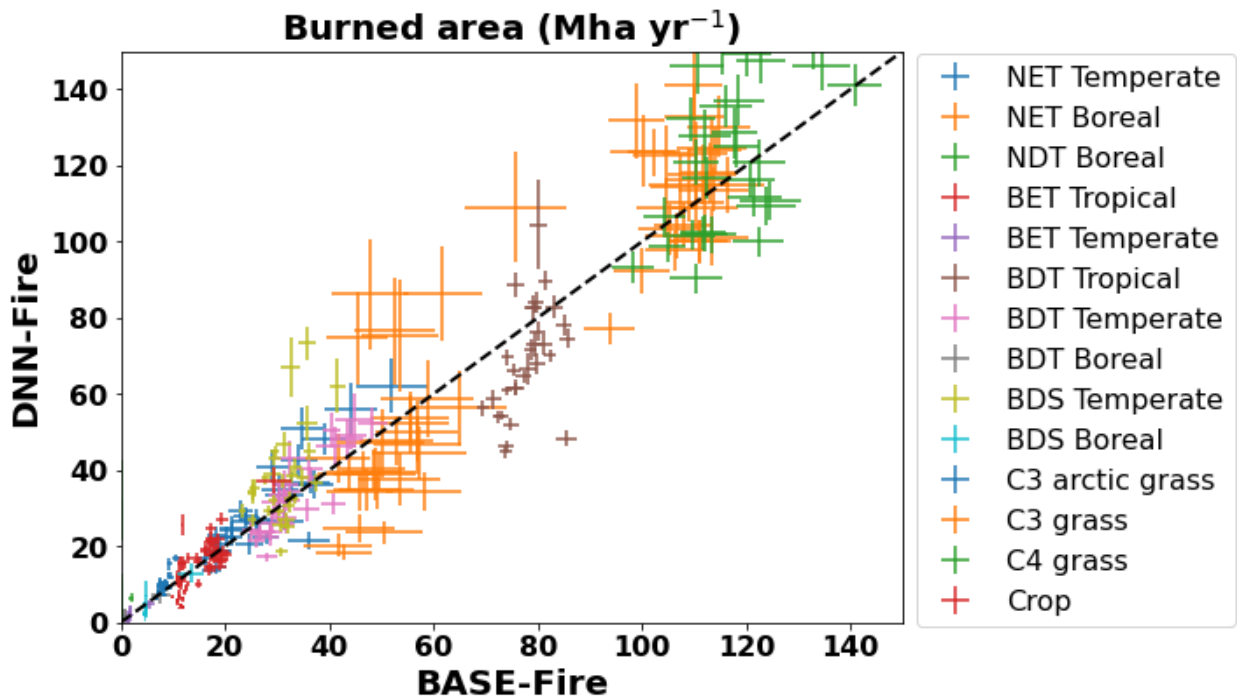
718
719
720

Figure S5. Sensitivity of modeled burned area (2001-2010 long-term averaged) to climate forcings (including temperature, precipitation, wind speed, relative humidity) and soil moisture.

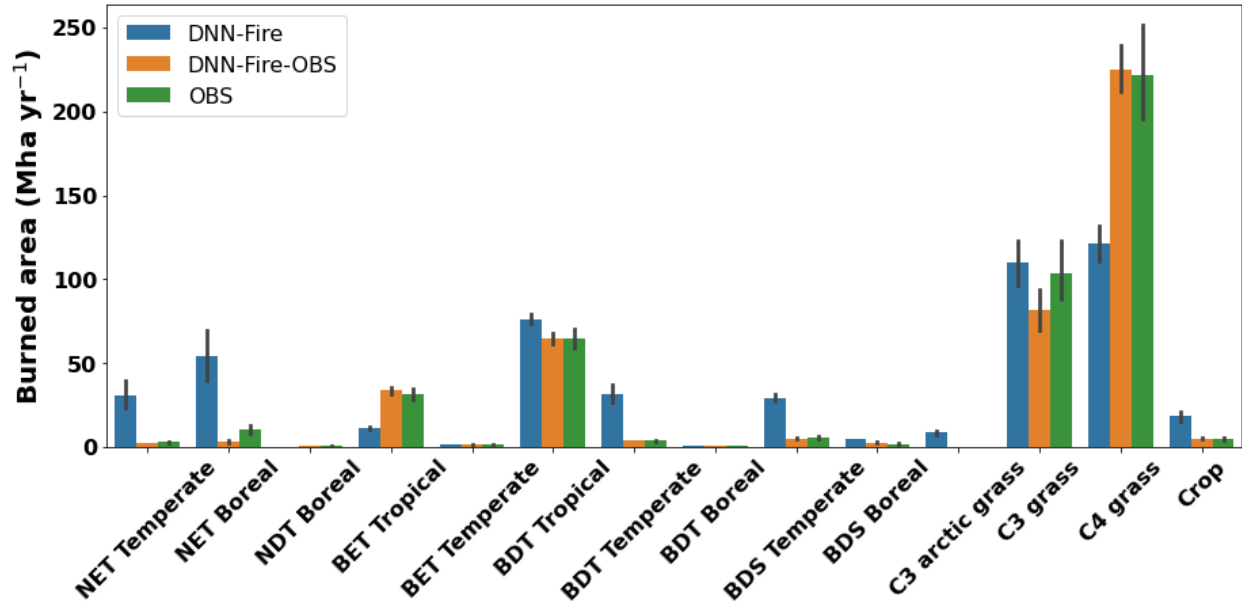
721 X-axis was burned area simulated by the default model using GSWP3 climate forcing and
 722 ELMv1 simulated soil moisture. Y-axis were models with alternative climate forcing (CRUJRA,
 723 NCEPDOE2) and soil moisture product (NCEP CDAS soil moisture).
 724
 725



726
 727 **Figure S6.** 3SM simulated global vegetation biomass [425-472 PgC] and observational based
 728 estimate of present-day living biomass (455 PgC GEOCARBON).
 729



730
 731 **Figure S7.** The performance of the Deep Neural Network wildfire model (DNN-Fire), compared
 732 with the original ELMv1 process-based wildfire model (BASE-Fire) aggregated over 14 plant
 733 functional types between years 2001 and 2010.
 734
 735



736
737
738
739
740

Figure S8. A comparison of wildfire burned area among Deep Neural Network wildfire model (DNN-Fire), Deep Neural Network wildfire model fine-tuned with observed burned area (DNN-Fire-OBS), and observations for 14 plant functional types.